

# HIGH-ORDER WENO SCHEMES ON UNSTRUCTURED TETRAHEDRAL MESHES

J. Rokicki\*, R. Wieteska†

Warsaw University of Technology,  
Institute of Aeronautics and Applied Mechanics  
Nowowiejska 24, 00-665 Warsaw, Poland  
e-mail: [\[jack,wietek\]@meil.pw.edu.pl](mailto:[jack,wietek]@meil.pw.edu.pl)

**Key words:** high order methods, irregular meshes, transonic flows

**Abstract.** *The paper discusses finite volume WENO reconstruction applied to simulation of compressible 3D Euler flows using unstructured tetrahedral meshes.*

*The main point of interest is the case when the mesh becomes highly irregular or stretched. Special transformation is used in such cases to recover the third-order accuracy of reconstruction. This transformation has to be locally applied to each stencil on which the reconstruction is sought. This procedure is verified first on a sequence of 3D meshes in a unit cube.*

*The performance of the full algorithm (including the extended nonlinear weighing) is verified for the 3D subsonic and transonic flows in a channel with smooth sinusoidal bump.*

## 1 INTRODUCTION

Finite Volume method provides straightforward conservative discretisation for Euler equations. In its basic form the control volumes coincide with grid cells, while the unknowns are located at the cell centers (cell-centered approach). In order to calculate fluxes at the cell walls, the solution is reconstructed within each cell using the information from its neighbourhood.

The order of spatial discretisation depends on two factors:

- the order of reconstruction within the cell,
- the order of integration formula used at the cell walls to calculate fluxes.

Higher order reconstruction coupled with WENO (Weighted Essentially Non Oscillatory method) was already considered in [1],[2],[3],[5].

In this paper however we investigate in more detail the possibility to obtain higher (third) order reconstruction of the solution on irregular/stretched triangular/tetrahedral meshes.

## 2 EULER EQUATIONS

The Euler model of fluid is used in the present paper. The equations in conservative form can be expressed as:

$$\frac{\partial U}{\partial t} + \nabla \cdot \mathcal{F}(U) = 0 \quad (1)$$

$$U = \begin{bmatrix} \rho \\ \mathbf{m} \\ \varepsilon \end{bmatrix}; \quad \mathbf{m} = \rho \mathbf{V}; \quad \mathcal{F}(U) = \begin{bmatrix} \mathbf{m}^T \\ \frac{1}{\rho} \mathbf{m} \otimes \mathbf{m} + p \mathbf{I} \\ H \mathbf{m}^T \end{bmatrix}$$

$$p = (\gamma - 1) \left( \varepsilon - \frac{\mathbf{m}^T \mathbf{m}}{2\rho} \right), \quad H = \frac{\gamma \varepsilon}{\rho} - (\gamma - 1) \frac{\mathbf{m}^T \mathbf{m}}{2\rho}$$

where:

$\rho$  - density

$\mathbf{V} = [u, v, w]$  - velocity vector

$\varepsilon$  - total energy per unit volume

$p$  - pressure

$H$  - total enthalpy

$\gamma = \frac{c_p}{c_v}$  - the ratio of specific heat capacities.

## 3 FINITE VOLUME DISCRETIZATION AND THE WENO ALGORITHM

After integration over the control volume  $\Omega_h$  the Euler equations become:

$$\frac{d}{dt} \int_{\Omega_h} U d\Omega = - \int_{\partial\Omega_h} \mathcal{F}(U) \cdot \mathbf{n} ds \quad (2)$$

The control volume  $\Omega_h$  has tetrahedral shape and its boundary consists of triangular faces  $\Gamma_1, \dots, \Gamma_4$  ( $\partial\Omega_h = \Gamma_1 \cup \dots \cup \Gamma_4$ ). Thus the right hand side of the equation (2) can be modified to:

$$\int_{\partial\Omega_h} \mathcal{F}(U) \cdot \mathbf{n} ds = \sum_j \int_{\Gamma_j} \mathcal{F}(U) \cdot \mathbf{n}_j ds \quad (3)$$

The integral over the triangular cell face  $\Gamma$  (with vertices  $\mathbf{r}_A, \mathbf{r}_B, \mathbf{r}_C$ ) is usually approximated by:

$$\int_{\Gamma} f(\mathbf{r}) d\sigma = |\Gamma| f(\mathbf{r}_0) \quad \mathbf{r}_0 = \frac{\mathbf{r}_A + \mathbf{r}_B + \mathbf{r}_C}{3} \quad (4)$$

( $f$  denotes arbitrary function, while  $|\Gamma|$  stands for the triangle area). This formula is second order accurate - which means that it is exact for linear polynomials. In order to increase accuracy we use third order formula (exact for up to quadratic polynomials):

$$\int_{\Gamma} f(\mathbf{r}) d\sigma = \frac{|\Gamma|}{3} \left( f\left(\frac{\mathbf{r}_A + \mathbf{r}_0}{2}\right) + f\left(\frac{\mathbf{r}_B + \mathbf{r}_0}{2}\right) + f\left(\frac{\mathbf{r}_C + \mathbf{r}_0}{2}\right) \right) \quad (5)$$

The flux in equation (2) is thus evaluated using  $U$  at the point of the cell face rather than using the value stored at the cell center. Therefore reconstruction step has to be performed to obtain distribution of  $U$  within each cell.

This mechanism will be illustrated for the standard second-order reconstruction and for an arbitrary scalar function  $\varphi$ . In this case linear distribution is assumed within each cell:

$$\varphi(\mathbf{r}) = \varphi(\mathbf{r}_0) + \mathbf{G}^T (\mathbf{r} - \mathbf{r}_0) \quad (6)$$

where  $\mathbf{r}_0$  denotes its center of gravity, while  $\mathbf{G}$  (evaluated using data from neighbouring cells) is a first-order approximation of  $\nabla\varphi$  at  $\mathbf{r}_0$ .

The original function  $\varphi(\mathbf{r})$  may contain discontinuities, thus nonlinear weighting has to be applied to suppress oscillation.

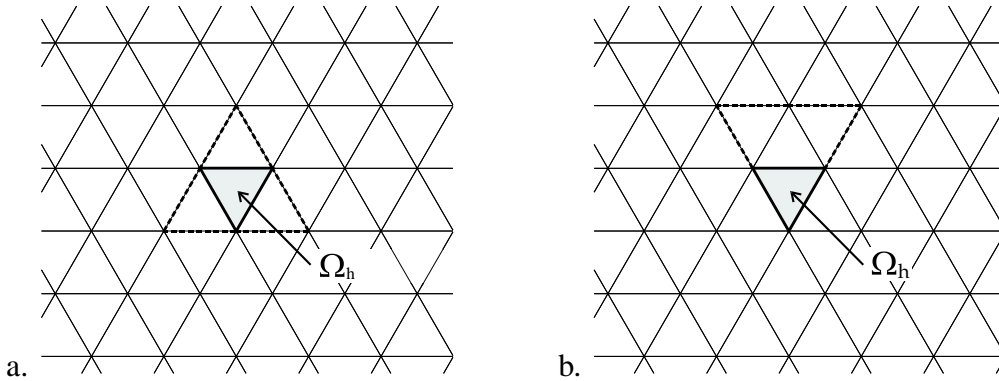


Figure 1: Stencils that can be used in 2D WENO reconstruction.

In multidimensional case this is done by the following typical WENO [3] algorithm:

- For a control volume  $\Omega_h$  stencils  $S_1, S_2, \dots, S_m$  are defined consisting of the neighbouring control volumes (Fig. 1 illustrates the 2D case).
- The value of gradient  $\mathbf{G}^\alpha$  is approximated on each stencil  $S_\alpha$
- The oscillation indicator  $o_\alpha$  and nonlinear weight  $\omega_\alpha$  are calculated for each stencil  $S_\alpha$

The resulting gradient is obtained as:

$$\mathbf{G}_{\text{WENO}} = \sum_{\alpha=1}^m \omega_{\alpha} \mathbf{G}^{\alpha} \quad (7)$$

where the oscillation indicator for linear reconstruction is defined as:

$$o_{\alpha} = \|\mathbf{G}^{\alpha}\|_2 \quad (8)$$

while the weights are assumed in the form:

$$\omega_{\alpha} = \frac{(\epsilon + o_{\alpha})^{-4}}{\sum_{i=1}^m (\epsilon + o_{\alpha})^{-4}} \quad (9)$$

In the above  $\epsilon \approx 10^{-6}$  is a small number introduced to eliminate problems in areas where  $\|\mathbf{G}\| \approx 0$  (e.g., near stagnation points).

#### 4 THIRD-ORDER RECONSTRUCTION

The procedure described in the previous Section has to be extended to higher-order discretisation. For this purpose suppose that  $\mathbf{r}_p$  ( $p = 0, \dots, m$ ) form a cloud of points on which function values  $\varphi_p = \varphi(\mathbf{r}_p)$  are prescribed.

We seek the reconstruction function in the form:

$$\varphi(\mathbf{r}) = \varphi_0 + \mathbf{G}^T (\mathbf{r} - \mathbf{r}_0) + \frac{1}{2} (\mathbf{r} - \mathbf{r}_0)^T \mathbf{H} (\mathbf{r} - \mathbf{r}_0) \quad (10)$$

where  $\mathbf{G}$  and  $\mathbf{H}$  stand for approximated gradient vector and Hessian matrix respectively. To obtain third order accuracy,  $\mathbf{G}$  and  $\mathbf{H}$  have to be estimated with second and first order accuracy respectively.

To achieve this goal both  $\mathbf{G}$  and  $\mathbf{H}$  are expressed as as linear combinations of the function increments:

$$\mathbf{G} = \sum_{p=1}^m \mathbf{G}_p w_p (\varphi_p - \varphi_0), \quad \mathbf{H} = \sum_{p=1}^m \mathbf{H}_p \bar{w}_p (\varphi_p - \varphi_0) \quad (11)$$

where vector coefficients  $\mathbf{G}_p$  and matrix coefficients  $\mathbf{H}_p = \mathbf{H}_p^T$  are unknown, while weights  $w_p = \|\mathbf{r}_p - \mathbf{r}_0\|^{-1}$ ,  $\bar{w}_p = \|\mathbf{r}_p - \mathbf{r}_0\|^{-2}$  are chosen such, that  $\mathbf{G}_p$  and  $\mathbf{H}_p$  become "dimensionless". These unknown coefficients can be found by expanding  $\varphi_p - \varphi_0$  in Taylor series:

$$\varphi_p - \varphi_0 = \mathbf{r}_{p0}^T \nabla \varphi \Big|_0 + \frac{1}{2} \mathbf{r}_{p0}^T \nabla^2 \varphi \Big|_0 \mathbf{r}_{p0} + O(h^3) \quad (12)$$

and by substituting (12) into (11), which results in the following expression:

$$\mathbf{G}(\varphi) = \sum_{p=1}^m \mathbf{G}_p \omega_p \mathbf{r}_{p0}^T \nabla \varphi \Big|_0 + \sum_{p=1}^m \mathbf{G}_p \omega_p \mathbf{r}_{p0}^T \nabla^2 \varphi \Big|_0 \mathbf{r}_{p0} \quad (13)$$

In the above  $\nabla^2 \varphi$  denotes Hessian matrix, while  $\mathbf{r}_{p0} = \mathbf{r}_p - \mathbf{r}_0$ .  
Our goal is to obtain:

$$\mathbf{G}(\varphi) \equiv \nabla \varphi \Big|_0 + O(h^2) \quad (14)$$

Thus the following equation system (compare (14) and (13)) must be fulfilled:

$$\forall \mathbf{v} \in \mathcal{R}^N \quad \sum_{p=1}^m \mathbf{G}_p \omega_p \mathbf{r}_{p0}^T \mathbf{v} = \mathbf{v} \quad (15)$$

$$\forall \mathbf{E} = \mathbf{E}^T \in \mathcal{R}^{N \times N} \quad \sum_{p=1}^m \mathbf{G}_p \omega_p \mathbf{r}_{p0}^T \mathbf{E} \mathbf{r}_{p0} = 0 \quad (16)$$

where  $N$  denotes the space dimension ( $N=2$  or  $3$ ). This equation system contains  $n = N + N \cdot (N + 1)/2$  equations and in general is underdetermined ( $n < m$ ). Similar system can be written to obtain approximate Hessian matrix. Both can be solved (separately) in a least-square sense minimising the solution norm. Numerically this is accomplished by applying sequence of Householder transformations.

The procedure, however, works well and delivers prescribed order of accuracy only if the cloud of points is sufficiently regular. This problem will be illustrated in the next Section.

## 5 THIRD-ORDER RECONSTRUCTION ON IRREGULAR MESHES

For the purpose of numerical experiment we introduce the transformation (in 3D):

$$\mathbf{r}^\eta = \begin{bmatrix} 1 & 0 & 0 \\ 0 & 1 & 0 \\ 0 & 0 & \eta \end{bmatrix} \cdot \mathbf{r} \quad \eta < 1. \quad (17)$$

which stretches the mesh (or cloud of points) in one direction (see Fig. 2 for 2D illustration). In the numerical experiment we take consecutive transformed meshes (for  $\eta = 2^0, 2^{-1}, 2^{-2}, \dots$ ) and calculate approximation  $\varphi(\mathbf{r})$  (10). The approximation error is obtained by subtracting the exact value of the benchmark function:

$$\varphi_*(\mathbf{r}) = \sin(x^2 + 2y^2 + z^2 + xy + 2yz + 4)$$

Additionally a sequence of 3D meshes (characterised by the average cell size  $h$ ) is taken to estimate the convergence characteristics of the scheme (see Fig. 3).

The results presented in Fig. 4 show already for  $\eta = 1/32$ , that not only the third-order of accuracy is lost, but also the absolute level of error increases.



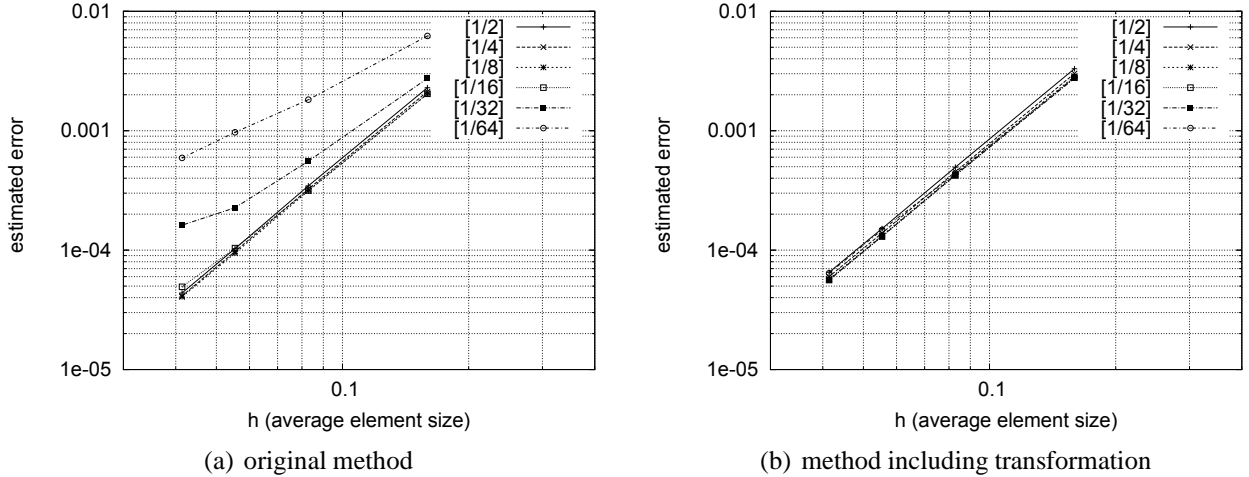


Figure 4:  $\|L\|_1$  extrapolation error (stretching factor  $\eta = 1/2, 1/4, \dots, 1/64$ ).

- the condition number of the underdetermined linear system (15– 16) grows roughly as  $\eta^{-3}$  (the condition number denotes the ratio of the largest and smallest modulus of all singular values)
- the weights introduced in formulas (11) do not reflect the directional information present in the cloud of points (the weights should rather be tensors than scalars).

The first, purely numerical factor is not the decisive one, which was verified using MAPLE™ high-precision computations (up to 100 significant digits).

However both problems can be alleviated by applying local transformation of the cloud of points used for approximation (the use of tensor weights in (11) might prove difficult).

This transformation is defined, with the help of the special matrix:

$$\mathbf{M} = \mathbf{M}[\mathbf{r}_0, \dots, \mathbf{r}_m] = \frac{1}{m+1} \sum_{p=0}^m \mathbf{r}_{pc} \cdot \mathbf{r}_{pc}^T \tag{18}$$

$$\mathbf{r}_{pc} = \mathbf{r}_p - \mathbf{r}_c, \quad \mathbf{r}_c = \frac{1}{m+1} \sum_{p=0}^m \mathbf{r}_p$$

which well characterised the anisotropy of the cloud. In particular  $\mathbf{M} = \mathbf{I}$  for sufficiently regular cloud (e.g., when symmetric vertices are located on the unit sphere).

The matrix  $\mathbf{M}$  is strictly positive when the cloud has full space dimension ( $\forall \mathbf{v}, \mathbf{v}^T \mathbf{M} \mathbf{v} > 0$ ), and in such case new matrices  $\mathbf{M}^{1/2}$  and  $\mathbf{M}^{-1/2}$  are well defined. Numerically  $\mathbf{M}^{1/2}$  and  $\mathbf{M}^{-1/2}$  are easily evaluated by the stable variant of the Newton algorithm [6] (p. 360). The regularising transformation is defined now by:

$$\mathbf{r}_{pc}^* = \mathbf{M}^{-1/2} \cdot \mathbf{r}_{pc} \quad (19)$$

It is straightforward to verify that the new cloud becomes isotropic since the new matrix:

$$\mathbf{M}^* = \mathbf{M}[\mathbf{r}_0^*, \dots, \mathbf{r}_m^*] = \mathbf{I}$$

On this transformed cloud both the gradient  $\mathbf{G}_*$  and the Hessian  $\mathbf{H}_*$  can be evaluated using the procedures introduced in Section 4.

The original gradient and Hessian can be recovered now as:

$$\mathbf{G} = \mathbf{M}^{1/2} \cdot \mathbf{G}_* \quad \mathbf{H} = \mathbf{M}^{1/2} \cdot \mathbf{H}_* \cdot \mathbf{M}^{1/2} \quad (20)$$

This two-step procedure proved to be successful even for highly stretched meshes ( $\eta \sim 2^{-6}$ ), which can be observed in Fig. 4(b).

## 6 NONLINEAR WEIGHTING

The nonlinear weighting described by (7) - (9) is extended to higher-order by the observation that the WENO first-order gradient  $\mathbf{G}_{\text{WENO}}$  (7) and the second-order gradient  $\mathbf{G}_{\text{II}}$  (11) should differ for the smooth fields by the first-order term:

$$\|\mathbf{G}_{\text{WENO}} - \mathbf{G}_{\text{II}}\|_2 \sim \bar{C} \cdot h \quad (21)$$

where  $h$  is the local cell size. The constant  $\bar{C}$  is then related to the norm of the Hessian (second derivative). The ratio:

$$C = \frac{\|\mathbf{G}_{\text{WENO}} - \mathbf{G}_{\text{II}}\|_2}{h} \quad (22)$$

is therefore used to design a continuous switching function allowing to reduce the approximation order in the neighbourhood of discontinuity. It is assumed that  $C < C_{\text{MAX}}$  ( $C_{\text{MAX}} = 10$  in present computations) corresponds to the smooth field where third-order reconstruction is possible. Above this value standard WENO reconstruction is employed.

Therefore, gradient  $\mathbf{G}$  and Hessian  $\mathbf{H}$  in the formula (11) are calculated as:

$$\mathbf{G} = \theta \cdot \mathbf{G}_{\text{II}} + (1 - \theta) \cdot \mathbf{G}_{\text{WENO}}, \quad \mathbf{H} = \theta \cdot \mathbf{H}_I \quad (23)$$

where:

$$\theta = \exp[-\max(0, C - C_{\text{MAX}})^4]$$

while  $\mathbf{H}_I$  denotes the Hessian obtained with first-order accuracy.

## 7 NUMERICAL VERIFICATION

The performance of the full method was investigated for the compressible flow in the 3D channel with sinusoidal bump. The height, width and the length of the channel were 0.5, 0.4 and 2.0 respectively. The shape of the lower wall was described by the function

$$z_L(x) = \begin{cases} 0 & x \notin \langle 0, 1 \rangle \\ \frac{1}{10} \sin^2(\pi x) & x \in \langle 0, 1 \rangle \end{cases}$$

Three meshes were generated (A, B and C) containing 2620, 21915 and 160958 cells. Between consecutive meshes the cell size was halved (on average). Mesh B is shown in Fig. 5

The first comparison between the 2<sup>nd</sup> order WENO and the present 3<sup>rd</sup> order method was performed for the fully subsonic case (Ma=0.5 at the inlet).

Figure 7 shows the Mach isolines for both methods to illustrate, that the largest differences occur at the bottom wall where the second-order method produces spurious entropy. This is better visible in Fig 8 where total pressure loss

$$w = 1 - \frac{p_0}{p_{0\infty}}, \quad p_{0\infty} > p_0$$

is plotted for all 6 cases (3 meshes and 2 methods). It is well visible that significant improvement exists between standard WENO and the present 3<sup>rd</sup> order method. Standard WENO on mesh B behaves like 3<sup>rd</sup> order method on mesh A, while the 3<sup>rd</sup> order method on mesh C is an order of magnitude more accurate than the best result of standard WENO.

For the more difficult transonic flow (Ma=0.56) the shockwave extends across the full height of the channel.

In this case the total pressure loss (on the shock) is similarly predicted by both methods. However the third-order method delivers a shockwave which is significantly sharper (judging by the distribution of total pressure loss).

## 8 CONCLUSIONS

The paper deals with the cell-centred Finite-Volume WENO method, which was extended to third-order for unstructured tetrahedral (triangular) meshes. The algorithm to obtain the third-order reconstruction (including second-order gradient vector and first-order Hessian matrix) was presented basing on the general least-squares approach.

It was shown that this algorithm is successful for relatively regular meshes. For highly distorted (stretched) meshes the additional preprocessing step was required, consisting of local transformation of the computational stencil.

The performance of the reconstruction was numerically investigated for a prescribed benchmark function defined on a cube. A sequence of meshes was used to prove the recovery of the third-order accuracy also for highly stretched meshes.

In order to deal with discontinuous solutions, the nonlinear weighting (WENO type) algorithm was adapted to the present reconstruction method. The full algorithm was tested for both subsonic and transonic flows in the 3D channel with sinusoidal bump on the lower wall.

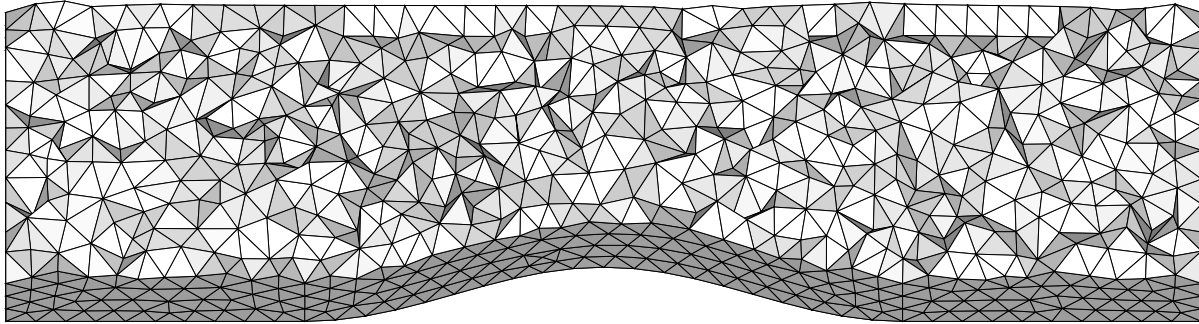


Figure 5: Grid B used for flow simulation (21915 cells, 3D cut for  $y=0.2$ , dark shading corresponds to the bottom wall).

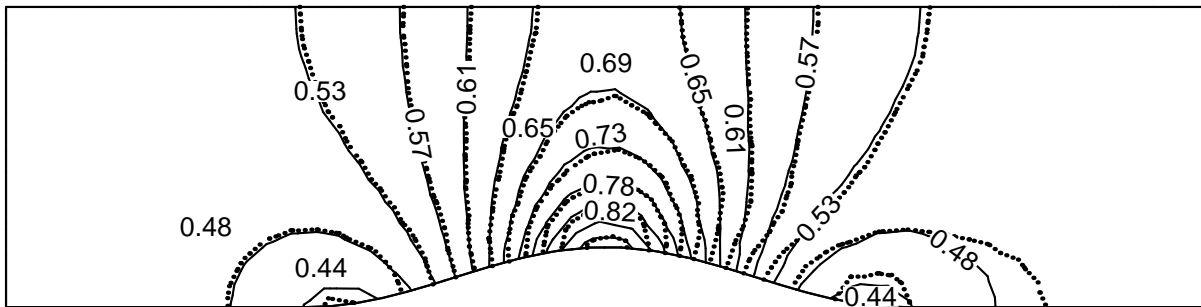


Figure 6: Mach isolines in 3D channel.  $Ma_{\text{inlet}} = 0.5$  (section  $y=0.2$ ), comparison of the  $3^{\text{rd}}$  order (solid line) and standard WENO (dotted line).

The subsonic results indicate that the presented third-order method significantly improves the accuracy of the solution in comparison with the standard second-order WENO method. This improvement of accuracy is largely obtained by reducing spurious entropy production on the wall. In the transonic case the third-order method provides thinner shock-waves (as judged by the pressure loss distribution) but otherwise the results are similar to those obtained by standard WENO.

Further investigation of the method is necessary, especially with respect to its behaviour near the solid walls. Additionally comparison should include results obtained by the Residual Distribution method.

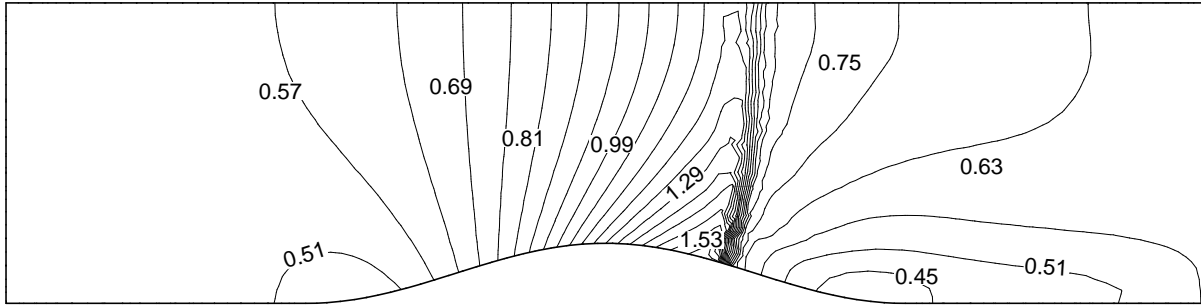
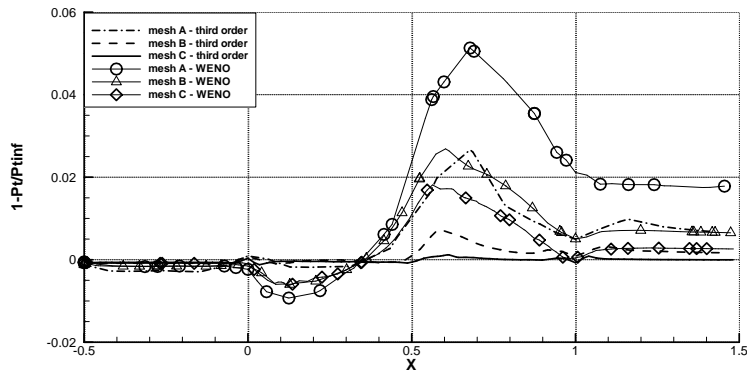
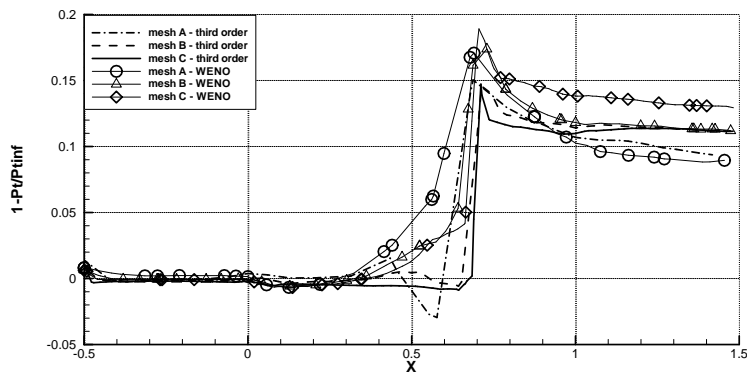


Figure 7: Mach isolines in 3D channel.  $Ma_{inlet} = 0.56$  (section  $y=0.2$ , mesh C).



(a)  $Ma=0.5$



(b)  $Ma=0.56$

Figure 8: Total pressure loss at the middle section of the channel.

## REFERENCES

- [1] F. Carl, Ollivier-Gooch. Quasi-ENO Schemes for Unstructured Meshes Based on Unlimited Data-Dependent Least-Squares Reconstruction. *Journal of Computational Physics*, **133**, 6–17, (1997).
- [2] J. Shi, Ch. Hu, Ch-W. Shu A Technique of Treating Negative Weights in WENO Schemes. *Journal of Computational Physics*, **175**, 108–127, (2002).
- [3] Ch. Hu, Ch-W. Shu. Weighted Essentially Non-oscillatory Schemes on Triangular Meshes. *Journal of Computational Physics*, **150**, 108–127, (2002).
- [4] R. Wieteska, J. Majewski, J. Rokicki. Investigation of WENO Schemes For 3D Unstructured Grids. *Computer Assisted Mechanics and Engineering Sciences*, (2006), (in print).
- [5] A. K. Henrick, T. D. Aslam, J. M. Powers. Mapped weighted essentially non-oscillatory schemes: Achieving optimal order near critical points. *Journal of Computational Physics*, **207**, 542–567, (2005).
- [6] M. Schatzman. Numerical Analysis - a mathematical introduction. *Clarendon Press - Oxford*, (2002).